A Counting Data Acquisition System for Measuring Parity Violation Asymmetry in Deep Inelastic Scattering

R. Subedi [a 1], D. Wang [a], K. Pan [b], X. Deng [a], R. Michaels [c], P. E. Reimer [d], A. Shahinyan [e], B. Wojtsekhowski [c], X. Zheng [a,*]

[a] *University of Virginia, Charlottesville, VA 22904, USA*
[b] *Massachusetts Institute of Technology, Cambridge, MA 02139, USA*
[c] *Thomas Jefferson National Accelerator Facility, Newport News, VA 23606, USA*
[d] *Argonne National Laboratory, Argonne, IL 60439, USA*
[e] *Yerevan Physics Institute, Yerevan, Armenia*

Abstract

An experiment that measured the parity violating asymmetry in deep inelastic scattering was completed at the Thomas Jefferson National Accelerator Facility in experimental Hall A. From this asymmetry one can extract a combination of the quark weak axial charge and improve over world data. To achieve this, asymmetries at the 10^{-4} level need to be measured. A specialized data acquisition (DAQ) system with intrinsic particle identification (PID) was developed and used. The DAQ system of this experiment is presented here with an emphasis on understanding of its PID performance, deadtime effect and the capability of measuring small asymmetries.

Key words: Jefferson Lab; Hall A; PVDIS; DAQ
PACS: 11.30.Er, 12.15.Mm, 13.60.Hb 14.60.Cd 14.65.Bt 29.30.Aj 29.85.Ca

[1] Present address: George Washington University, 725 21st St, NW, Washington, DC 20052, USA
[*] Corresponding author. E-mail: xiaochao@jlab.org; Telephone: 001-434-243-4032; Fax: 001-434-924-4576

1 Introduction

The Parity Violating Deep Inelastic Scattering (PVDIS) experiment E08-011 was completed in December 2009 at the Thomas Jefferson National Accelerator Facility (JLab). The goal of this experiment [1,2] was to measure to a high precision the parity violating asymmetry in deep inelastic scattering of a polarized electron beam on an unpolarized liquid deuterium target. This asymmetry is sensitive to a combination of the quark weak axial charge $2C_{2u} - C_{2d}$, where $C_{2q} = 2g_V^e g_A^q$ with $q = u, d$ indicating an up or a down quark, g_V^e is the electron vector coupling and g_A^q is the quark axial coupling to the Z^0 boson.

For electron inclusive scattering from an unpolarized target, the electromagnetic interaction is parity conserving and is insensitive to the spin flip of the incoming electron beam. Only the weak interaction violates parity. Taking the difference of the left- and right-handed electron scattering cross-sections, one can isolate the parity violating contribution. The parity violating asymmetry for deep inelastic electron scattering from a deuterium target, A_{PV}, can be written as

$$A_{PV} \equiv \frac{\sigma_R - \sigma_L}{\sigma_R + \sigma_L} = \left(-\frac{G_F Q^2}{4\sqrt{2}\pi\alpha}\right)\left(2g_A^e Y_1 \frac{F_1^{\gamma Z}}{F_1^{\gamma}} + g_V^e Y_3 \frac{F_3^{\gamma Z}}{F_1^{\gamma}}\right) , \tag{1}$$

where $\sigma_R(L)$ is the cross section for right-(left-)handed incident electrons, Q^2 is the negative of the four-momentum transfer squared, G_F is the Fermi weak coupling constant, α is the fine structure constant, Y_1 and Y_3 are kinematic factors, and x is the Bjorken scaling variable. In the quark parton model,

$$F_1^{\gamma Z} = \sum g_V^q Q_q \left[q(x) + \bar{q}(x)\right] \tag{2}$$
$$F_3^{\gamma Z} = \sum g_A^q Q_q \left[q(x) - \bar{q}(x)\right] \tag{3}$$
$$F_1^{\gamma} = \frac{1}{2}\sum Q_q^2 \left[q(x) + \bar{q}(x)\right] \tag{4}$$

where Q_q is the electric charge of quarks and $q(x)$, $\bar{q}(x)$ are quark distribution functions. Rewriting $g_{A(V)}^e g_{V(A)}^q$ as $C_{1(2)q}$, and assuming $R^{\gamma} = R^{\gamma Z} = 0$ where $R^{\gamma(Z)} = \sigma_L^{\gamma(Z)}/\sigma_T^{\gamma(Z)}$ is the ratio of the longitudinal to transverse cross section of the virtual photon exchange ($\gamma^* - Z$ interference), one has $Y_1 = 1$ and

$$A_{PV} = \left(\frac{3G_F Q^2}{\pi\alpha^2\sqrt{2}}\right) \times \frac{2C_{1u}[1 + R_C(x)] - C_{1d}[1 + R_S(x)] + Y_3(2C_{2u} - C_{2d})R_V(x)}{5 + R_S(x) + 4R_C(x)} , \tag{5}$$

where $R_{V,C,S}$ are related to quark distributions. The magnitude of the asymmetry is in the order of 10^{-4}, or 100 parts per million (ppm) at $Q^2 = 1$ (GeV/c)^2. The tree-level Standard Model effective weak coupling constants $C_{1,2q}$ are

$$C_{1u} = 2g_A^e g_V^u = -\frac{1}{2} + \frac{3}{4}\sin^2\theta_W \ , \ \ C_{2u} = 2g_V^e g_A^u = -\frac{1}{2} + 2\sin^2\theta_W \ ,$$
$$C_{1d} = 2g_A^e g_V^d = \frac{1}{2} - \frac{2}{3}\sin^2\theta_W \ , \ \ C_{2d} = 2g_V^e g_A^d = \frac{1}{2} - 2\sin^2\theta_W \ ,$$

with θ_W the weak mixing angle. The goal of JLab E08-011 is to measure the PVDIS asymmetries to statistical precisions of 3% and 4% at $Q^2 = 1.1$ and 1.9 (GeV/c)^2, respectively. In addition, the systematic uncertainty goal is $< 3\%$, and under the assumption that hadronic physics corrections are small, our goal is to extract from these asymmetries the effective coupling constant combination $(2C_{2u} - C_{2d})$. The magnitudes of the asymmetries are expected to be 90 and 170 ppm for the two measured kinematics of $Q^2 = 1.1$ and 1.9 (GeV/c)^2, respectively. To achieve the required precision, a rate capability of up to 500 kHz is needed. Although this is not the first time the PVDIS asymmetries are measured, the only preceding PVDIS measurement have been carried out at SLAC [3,4] in the late 1980's, with approximately 9% statistical and 9% systematic uncertainties. The increased precision of this experiment required better controls of all systematic uncertainties.

The experiment used a 100 μA polarized electron beam with a polarization of approximately 90% and a 20-cm long liquid deuterium target. The two High Resolution Spectrometers (HRS) [5] were used to detect scattered electrons. Similar to other deep inelastic scattering experiments, the main challenge of the measurement is to separate electrons from charged pion background due to electro- or photo-production. While the standard HRS detector package and data acquisition (DAQ) system routinely provide a good particle identification (PID), they are based on full recording of the detector signals and are limited to event rates up to 4 kHz. This is not sufficient for the high rates expected for the experiment. The HRS DAQ will be referred to as "standard DAQ" hereafter. For previous JLab parity violation experiments [7,8] focusing on elastic scattering from nuclear or nucleon targets, integrating DAQ could be used because elastic scattering typically is not contaminated by backgrounds. For the SLAC PVDIS experiment, an integrating DAQ was used with the input being the lead-glass detector signals. However, about 2% of the integrated signal was from the pion background. This would cause a systematic uncertainty comparable in size to our statistical uncertainty and a better data collection method must be found.

2 Detector and DAQ Overview

The design goal of the experiment is to record data up to 1 MHz with hardware-based PID and well measured and understood deadtime effects. The following detectors in the HRS were used: Two scintillator planes provided the main trigger, while a CO_2 gas Cherenkov detector and a double-layer segmented lead-glass detector provided particle identification information. The vertical drift chambers (as the tracking detector) were used during calibration runs and turned off during production data taking because they were not expected to endure the high event rates.

For the gas Cherenkov and the lead-glass detector, a full recording of their output ADC data is not feasible at the expected high rate. Instead their signals are passed through discriminators and logic units to form preliminary electron and pion triggers. Particle identification is fulfilled by the use of discriminators for both the lead-glass and the Cherenkov detectors and proper settings of their thresholds. These preliminary triggers are then combined with the scintillator triggers and Cherenkov signals to form the final electron and pion triggers, which are then sent to scalers to record the event counts and offline used to form asymmetries $A = (n_R - n_L)/(n_R + n_L)$, where $n_{R(L)}$ is the integrated rate of the triggers normalized to the integrated beam charge for the right(R) and left(L) handed spin states (helicity) of the incident electron beam. The scalers that count triggers and beam charge are integrated over the helicity period, which was flipped pseudo-randomly at 30 Hz per the experimental technique used by the HAPPEX experiments [9].

For HRS the two layers of the lead-glass detector are called “preshower” and “shower” detectors, respectively. The preshower blocks in the Right HRS (the spectrometer located to the right side of the beamline when viewed along the beam direction) has 48 blocks arranged in a 2×24 array, with the longest dimension of the blocks aligned perpendicular to the particle trajectory. For the two blocks in each row, only the ends facing outward are read out by photo-multiplier tubes (PMTs) and the other ends of the two blocks were facing each other and not read out. Therefore the preshower detector had 48 output channels. All preshower blocks were individually wrapped to prevent light leak. The preshower and the shower detectors in the Left HRS are similar to the preshower detector on the Right HRS except that for each detector there are 34 blocks arranged in a 2×17 array. The shower detector in the Right HRS had 75 blocks arranged in a 5×15 array with the longest dimension of the blocks aligned along the trajectory of scattered particles. PMTs are attached to each block of the Right shower detector on one end only, giving 75 output channels.

Because the lead-glass detectors in the Left and Right HRS were built differently, design of the lead-glass-based triggers of the DAQ is also different, as shown in Fig. 1. As a compromise between the amount of electronics needed and the rate in the front end logic modules, the lead-glass blocks in both the preshower and the shower detectors were divided into 6 (8) groups for the Left (Right) HRS, with each group consisting 8 blocks. On the Right HRS only 60 of the 75 shower blocks were used while the 15 blocks on the edge were not read out. The reduction on the HRS acceptance due to not using these side blocks is negligible. Signals from the 8 blocks in each group were added using a custom-made analog summing unit called

"SUM8 modules", then passed to discriminators. The geometry and the position of each pre-shower group was carefully chosen to match those of the corresponding shower group to maximize electron detection efficiency. On the Left HRS adjacent groups in both preshower and shower had overlapping blocks, while for the Right HRS only preshower blocks were overlapping. To allow overlap between adjacent groups, signals from preshower blocks on the Right HRS and from both preshower and shower blocks on the Left HRS were split into two identical copies using passive splitters.

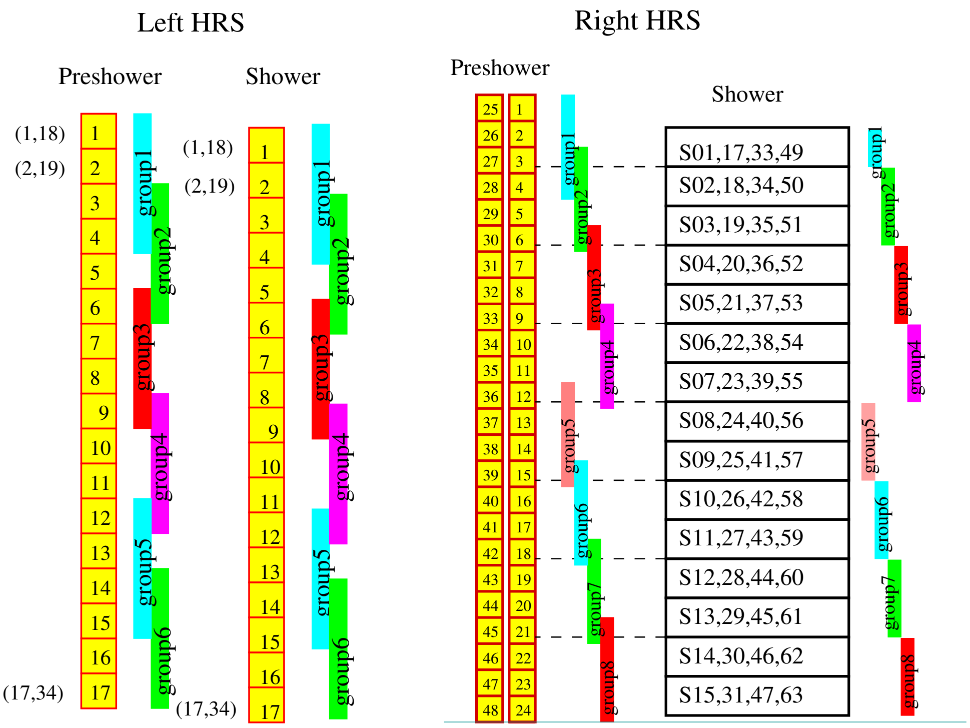

Fig. 1. [*Color online*] Grouping scheme (side-view) for the double-layer lead-glass detectors for the Left and the Right HRS. Scattered particles enter the detector from the left. The colored vertical bars represent the range of each group.

A schematic diagram for the DAQ electronics for the Right HRS is shown in Fig. 2. The electron and pion triggers were formed by passing shower (SS) and preshower (PS) signals or their sums, called total shower (TS) signals, through discriminators with different thresholds. For electron triggers, logical ANDs of the PS discriminator and the TS discriminator outputs were used. For pion triggers, low threshold discriminators on the TS signal alone were used to reject background. These signals were then combined with signals from scintillators and the gas Cherenkov (called electron or pion "VETO" signals) to form electron or pion triggers for each shower and preshower group. The electron VETO signals required the gas Cherenkov to be triggered, while the pion VETO required the opposite. The electron or pion triggers from all six groups on the Left HRS (eight groups for the Right HRS) were then ORed together to form the global electron or pion triggers for the Left (Right) HRS. All triggers – electron and pions from each group, as well as the final global triggers – were counted using scalers. Because pions do not produce large enough

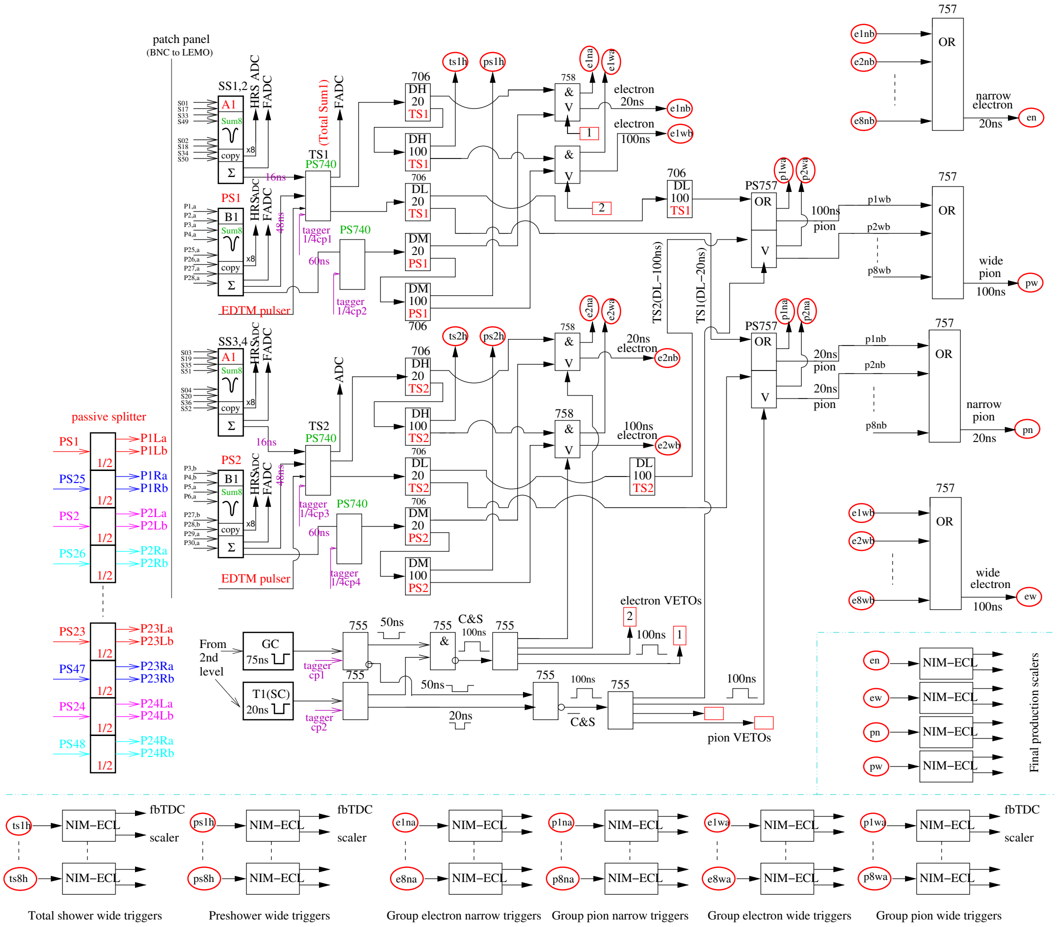

Fig. 2. [*Color online*] Electronics diagram for the Right HRS DAQ used by the PVDIS experiment. The Sum8's, discriminators and logic modules for two groups are shown, as well as the location of tagger signal inputs, setup of the VETO circuit using scintillator and gas Cherenkov signals, the logic units for combining triggers from all eight groups into final triggers, and the scalers. Electronics for the Left HRS are similar except for the grouping scheme.

lead-glass signals to trigger the high threshold TS discriminators for the electron triggers, pions do not introduce extra counting deadtime for the electron triggers.

In order to monitor the counting deadtime of the DAQ, two identical paths of electronics were constructed. The only difference between the two paths is in the discriminator output width, set at 30 ns and 100 ns for the "narrow" and the "wide" paths, respectively. The scalers are rated for 250 MHz (4 ns deadtime) and therefore do not add to the deadtime. In addition, since the output width of all logic modules were set to 15 ns, the deadtime of the DAQ for each group is dominated by the deadtime of the discriminators.

The SUM8 modules used for summing all lead-glass signals also served as fan-out modules, providing exact copies of the input PMT signals. These copies were sent to the standard HRS DAQ for calibration.During the experiment, data were collected at low rates using reduced beam currents with both DAQs functioning, such that a direct comparison of the two DAQs can be made. The vertical drift chambers were used during these low rate DAQ studies. Outputs from all discriminators, signals from the scintillator and the gas Cherenkov, and all electron and pion triggers were sent to Fastbus TDCs (fbTDC) and were recorded in the standard DAQ. Data from these fbTDCs were used to align amplitude spectrum and its timing. They also allow the study of the Cherenkov or lead-glass performance for the new DAQ triggers.

Full sampling of analog signals were done using Flash-ADCs (FADCs) at low rates intermittently during the experiment. For one group on the left and one group on the right HRS, the preshower and shower SUM8 outputs, the intermediate logical signals of the DAQ, and the output electron and pion triggers were recorded. These FADC data provide a study of pileup effects to confirm the simulation and to provide the input parameters for the simulation, specifically the rise and fall times of the signals and their widths.

3 DAQ PID Performance

PID performance of the DAQ system was studied with calibration runs taken at low beam currents using fbTDC signals along with ADC data of all detector signals recorded by the standard DAQ. Events that triggered the DAQ would appears as a timing peak in the corresponding fbTDC data of the standard DAQ and a cut on this peak can be used to select those events. Figure 3 shows the preshower vs. shower signals for group 2 on the Left HRS. A comparison between no fbTDC cut and with cut on the fbTDC signal of the electron wide trigger from this group clearly shows the hardware PID cuts.

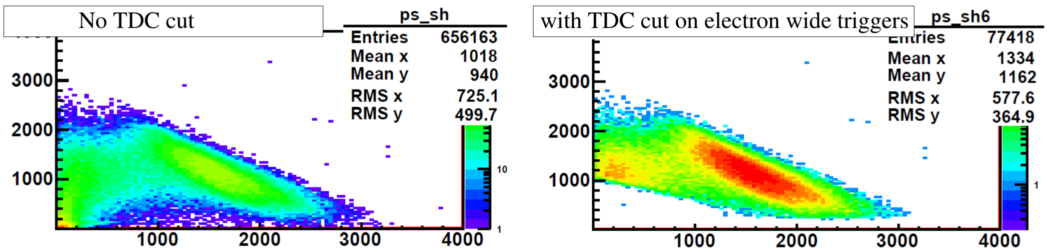

Fig. 3. [*Color online*] Preshower vs. Shower ADC data (sum of 8 blocks each) for group 2 on the Left HRS, without the fbTDC cut (left panel) and with cut on the group 2 electron wide trigger fbTDC signal (right panel). It clearly shows the thresholds on the preshower and the total shower signals, indicating the DAQ is selecting the correct events as electrons. The events near the vertical axis, around ADC channels (200,1000), are electrons that deposited energy in overlapping blocks between group 2 and group 1 (or group 3) and are recorded by the other group.

Electron efficiency and pion rejection factors of the lead-glass detector on the Left HRS are shown in Fig. 4 as functions of the location of the hit of the particle in the preshower detector. PID performance on the Right HRS is similar. Electron efficiency from wide groups are slightly higher than narrow groups because there is less event loss due to timing mis-alignment when taking the coincidence between the preshower and the total shower discriminator outputs. Variations in the electron efficiency across the spectrometer acceptance effectively influence the kinematics (Q^2) of the measurement. For this reason, low-rate calibration data were taken daily during the experiment to monitor the DAQ PID performance and corrections are applied to data.

Pion contamination in the electron trigger would affect the measured electron asymmetry as $A_e^m = (A_e^{\mathrm{true}} + fA_\pi)/(1+f)$ where A_e^m and A_e^{true} are the measured and the true electron asymmetries, respectively, f is the pion contamination fraction in the electron trigger, and A_π is the parity violation asymmetry of pion production. As shown in Fig. 4, pion rejection factor from the lead-glass detector was above 50. Combined with the approx. 200 pion rejection factor of the gas Cherenkov detector [5], the total pion rejection achieved during this experiment was above 10^4. The pion to electron rate ratios for the two Q^2 values of this experiment were less than 10:1, thus $f < 10/10^4 = 10^{-3}$. Because pions are produced from nucleon resonance decays, the parity violation asymmetry of pion production is expected to be no larger than that of scattered electrons with the same momentum. This was confirmed by asymmetries formed from pion triggers during this experiment. Overall the uncertainty in the electron asymmetry due to pion contamination is less than 10^{-3} and is negligible compared to the $3-4\%$ statistical uncertainty.

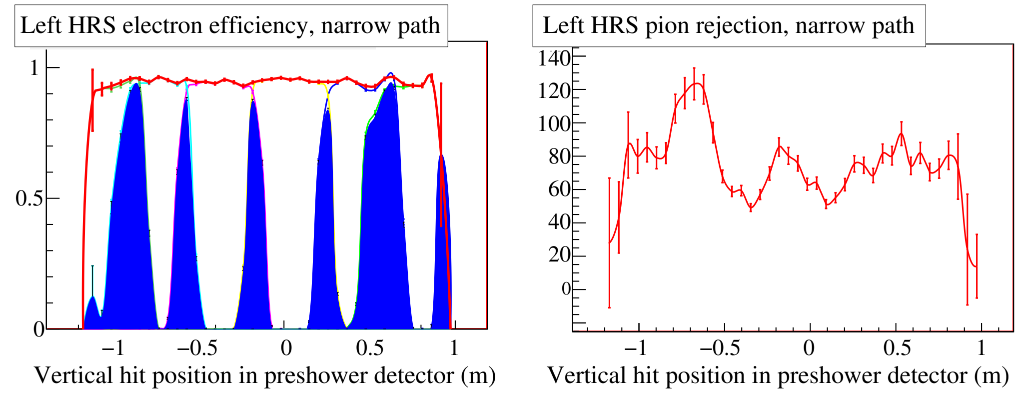

Fig. 4. [*Color online*] Electron detection efficiency (left) and pion rejection factor (right) vs. vertical (dispersive) hit position of the particle in the preshower detector for the narrow electron triggers in the Left HRS. A one-hour run was used in this evaluation. For electron efficiencies, the total efficiency is shown by the red curve, while blue shaded area indicates events that are recorded by the two adjacent groups. The average electron efficiency across the detector for this one-hour run is $(94.626 \pm 0.002)\%$ and the averge pion rejection factor is 75.3 ± 1.1. The error bars are statistical only. PID performance for the wide path and the Right HRS are similar.

4 DAQ Deadtime

Deadtime is the amount of time after an event during which the system is unable to record another event. Identifying the exact value of the deadtime is always a challenge in counting experiments. By having a narrow and wide path, we can observe the trend in the deadtime – the wider path should have higher deadtime. By matching the observed trend with our simulation we can benchmark and confirm the simulation result of our deadtime. In addition, dividing lead-glass blocks into groups greatly reduces the deadtime loss in each group compared to summing all blocks together and forming only one final trigger.

To illustrate the importance of the deadtime, consider its affect on the asymmetry A. For a simple system with only one contribution to the deadtime δ, the observed asymmetry A_O is related the the true asymmetry A according to $A_O = (1-\delta)A$. In this experiment δ was on the order of 0.02 (dependent on the rate). To achieve a 3% accuracy on the asymmetry, δ must be known with a $\leq 30\%$ relative accuracy, so that it becomes a negligible systematic error. The DAQ we deployed was, however, more complex, having the three contributions to the deadtime, as listed below and shown in Fig. 2:

(1) The "group" deadtime: deadtime due to discriminators and logical AND modules used to form group triggers;
(2) The "veto" deadtime: deadtime from electronics that used scintillator and Cherenkov signals to form the "gate" signals which were sent to the AND module of each group to form group electron and pion triggers.
(3) The "OR" deadtime: deadtime due to the logical OR module when combining all group triggers.

The final deadtime is a combination of all three. In order to evaluate the DAQ deadtime, a full-scale simulation was developed as follows: The analog signals for preshower, shower, scintillator and gas Cherenkov as recorded by ADCs from low-current runs are fed to the simulation as inputs. The simulation takes into account all electronics and delay cables of the DAQ and calculate digital outputs from discriminators, all AND and OR modules. For the preshower and shower SUM8 outputs, FADC data were used to determine the signal width.

4.1 Group Deadtime Measurement

In order to study the group deadtime, a high rate pulser signal ("tagger") was mixed with all preshower and total shower signals using analog summing modules, see Figs. 2 and 5. In the absence of all detector signals, a tagger pulse produces without loss an electron trigger output, and a "tagger-trigger coincidence" pulse between this output and the delayed tagger – the tagger itself with an appropriate delay to account for the DAQ response time. When high-rate detector signals are present, however, some of the tagger would not be able to trigger the DAQ due to deadtime. The relative loss in the tagger output w.r.t. the tagger input has two components:

(1) The count loss R_o/R_i: when a detector PMT signal precedes the tagger signal by a time interval δt shorter than the DAQ deadtime but longer than the delayed tagger pulse width, the tagger signal is lost and no coincidence output is formed;
(2) The pileup fraction p: when a PMT signal precedes the tagger signal by a time interval δt shorter than the delayed tagger signal width, there would be coincidence output between the delayed tagger and the electron output triggered by the detector PMT signal. If δt is less than the DAQ deadtime (which is true for this experiment), the tagger itself is lost due to deadtime and the tagger-trigger coincidence is a false count and should be subtracted. In the case if δt is longer than the DAQ deadtime (not true for this experiment but could happen in general), the tagger itself also triggers a tagger-trigger coincidence but in this case, there are two tagger-trigger coincidence events, both recorded by the fbTDC if working in the multi-hit mode, and one is a false count and should be subtracted.

    The pileup effect can be measured because the delay between the coincidence output and the input tagger would be smaller than when the electron output is caused by the tagger. This effect is illustrated in Fig. 5 and contributes to both I_1 and I_2 region of the fbTDC spectrum. Fractions of I_1 and I_2 relative to I_0 are expected to be $I_1/I_0 = Rt_1$ and $I_2/I_0 = Rw$, respectively, where R is the PMT signal rate, w is the width of the trigger output and t_1 is the time interval the delayed tagger precedes the tagger's own trigger output. During the experiment w was set to 15 ns for all groups, t_1 was measured at the end of the experiment and was found to be between 20 and 40 ns. Data for $I_{1,2}$ extracted from fbTDC agree very well with the expected values.

The fractional loss of tagger events due to DAQ deadtime is evaluated as

$$D = 1 - (1 - p)(R_o/R_i), \tag{6}$$

where R_i is the *i*nput tagger rate, R_o is the *o*utput tagger-trigger coincidence rate, and $p = (I_1 + I_2)/I_0$ is a correction factor for pileup effects (see Fig. 5 for definition of $I_{0,1,2}$). The pileup effect was measured using fbTDC spectrum for electron narrow and wide triggers for all groups. Results for the deadtime loss D are shown in Figs. 6 and 7 and compared with simulation. Different beam currents between 20 and 100 μA were used in this dedicated deadtime measurement. In order to reduce the statistical fluctuation caused by limited number of trials in the simulation within a realistic computing time, simulations were done at higher rates than the actual measurement.

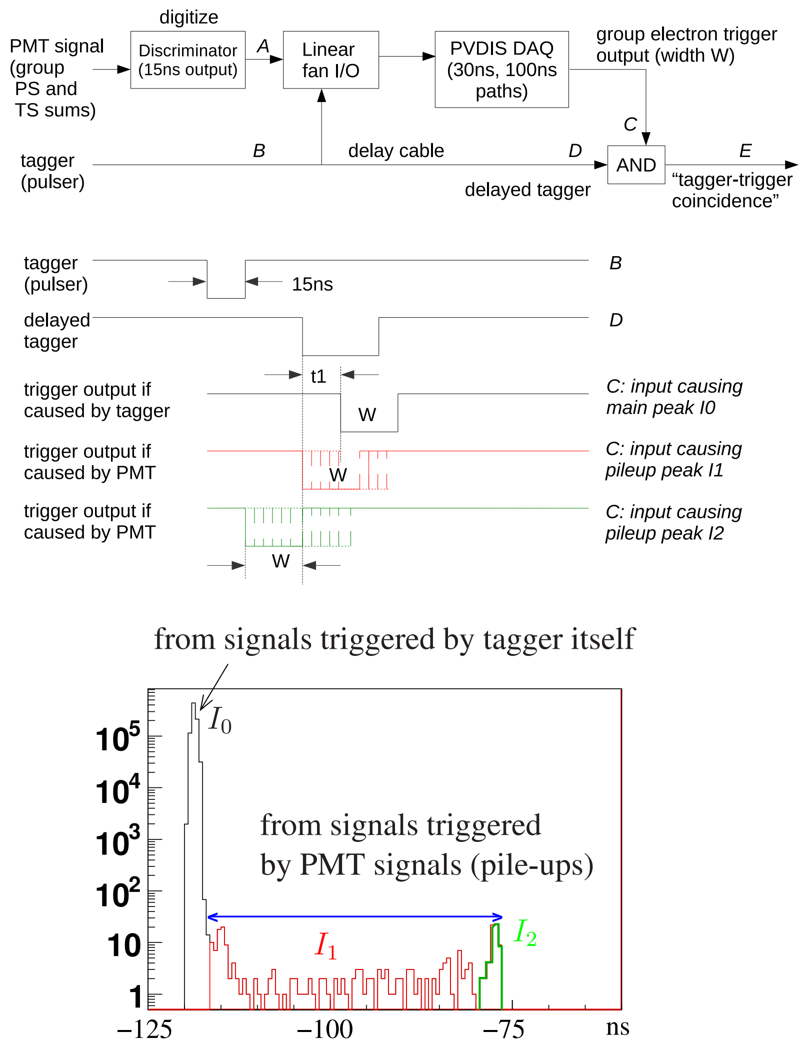

Fig. 5. [*Color online*] Top: schematic diagram for the tagger setup and signal timing sequence. Bottom: fbTDC spectrum for the relative timing between tagger-trigger coincidence and the input tagger, in 0.5-ns bins. The fbTDC module works in the multi-hit mode. Two different scenarios are shown: 1) Main peak I_0: when there is no PMT signal preceding the tagger, the tagger triggers the DAQ and forms a tagger-trigger coincidence. 2) Pileup events I_1 and I_2: when there is a PMT signal preceding the tagger by a time interval shorter than the delayed tagger width, the PMT signal triggers the DAQ and forms a tagger-trigger coincidence signal with the delayed tagger.

The slope of the tagger loss vs. event rate gives the value of group deadtime in seconds, as shown in Figs. 6 and 7, for group 4 on the left HRS and group 4 on the right HRS, respectively. These data are compared with results from the simulation. One can see that the deadtime for the wide path is approximately 100 ns as expected. The deadtime for the narrow path, on the other hand, is dominated by the input PMT signal width (typically 60-80 ns) instead of the 30-ns discriminator width. The simulated deadtime agree very well than data for both HRSs and for

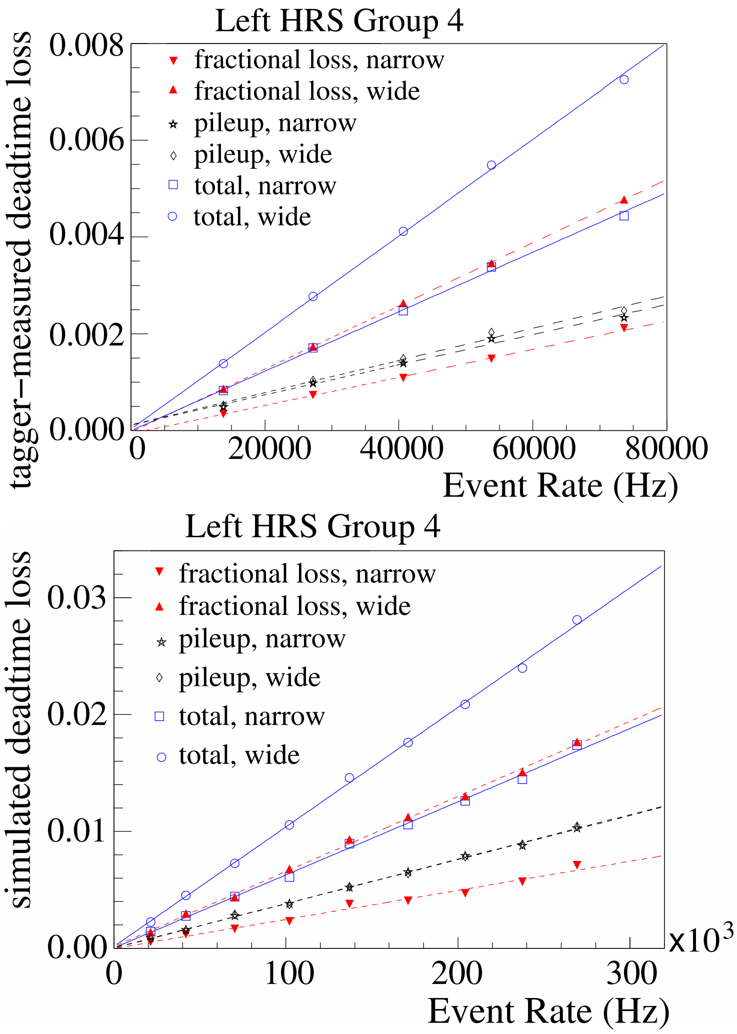

Fig. 6. [*Color online*] Deadtime loss in percent vs. event rate from the tagger method for group 4 on the Left HRS. Top: actual deadtime loss from tagger measurements; Bottom: simulated deadtime loss of the tagger. The tagger fractional count loss $1 - R_o/R_i$ (red) and the pileup correction p (black) are combined to form the total group deadtime D (blue). These data were taken (or simulated) at a Q^2 of 1.1 (GeV/c)^2. To minimize the statistical uncertainty while keeping the computing time reasonable, the simulation used higher event rates than the tagger measurement. The total group deadtime can be determined from the linear fit slope coefficients: tagger data narrow $p_1 = (61.5 \pm 0.2) \times 10^{-9}$ s, wide $p_1 = (99.9 \pm 0.3) \times 10^{-9}$ s, simulation narrow $p_1 = (62.5 \pm 1.4) \times 10^{-9}$ s, wide $p_1 = (102 \pm 1.3) \times 10^{-9}$ s. Group 4 is from the central blocks of the lead-glass detector and has the highest rate among all groups.

both wide and narrow paths.

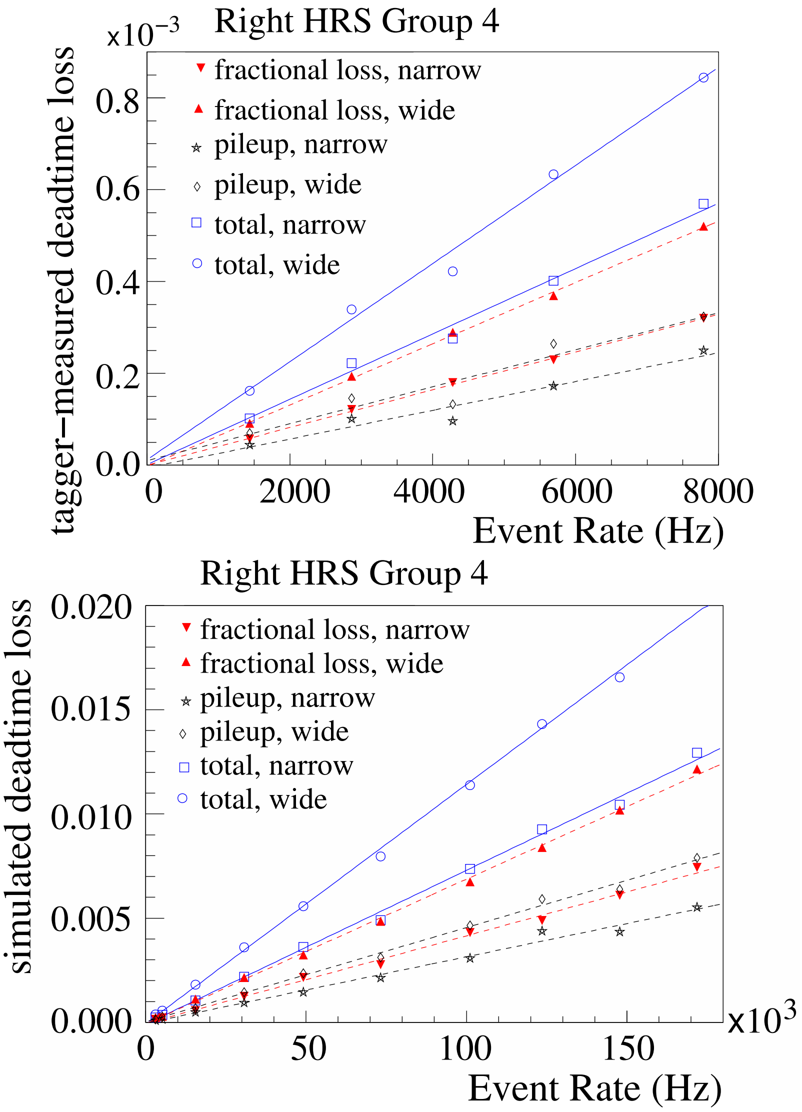

Fig. 7. [*Color online*] Deadtime loss in percent vs. event rate from the tagger method for group 4 on the Right HRS. Top: tagger data; Bottom: simulation. These data were taken (or simulated) at a Q^2 of 1.9 (GeV/c)^2. The total group deadtime can be determined from the linear fit slope coefficients: tagger data narrow $p_1 = (71.1 \pm 0.9) \times 10^{-9}$ s, wide $p_1 = (107 \pm 1.2) \times 10^{-9}$ s, simulation narrow $p_1 = (73.9 \pm 1.5) \times 10^{-9}$ s, wide $p_1 = (115 \pm 1.5) \times 10^{-9}$ s. Group 4 is from the central blocks of the lead-glass detector and has the highest rate among all groups. See Fig. 6 caption for details.

4.2 Total Deadtime Evaluation

Although the deadtime loss of each group was measured using tagger signals, the dominating term in the total deadtime is from the veto electronics because the total trigger rate from scintillators and gas Cherenkov is much higher than individual group rates. The difference in total loss between narrow and wide path is thus smaller than that in their group deadtimes. Simulation for the veto deadtime was compared with FADC data and the agreement was found to be at 20% level or better. After subtracting group and veto deadtimes from the total simulated deadtime, the remaining is attributed to the logical OR module. There is no direct measurement of the logical OR deadtime, but the effect of the logical OR module is quite straightforward and can be calculated analytically. The difference between the simulation and the analytic results can be used to estimate the uncertainty of the OR deadtime.

The simulated deadtime loss of the global electron triggers and its decomposition into group, veto, and OR are shown in Table 1. The total deadtime is also shown in Fig. 8 as a function of the total event rate. The deadtime corrections to

Table 1
Simulated DAQ deadtime loss (in percent) and fractional contributions from group, veto, and OR deadtimes. The fractional deadtime from OR is calculated as one minus those from group and veto, and its uncertainty is estimated from the difference between simulation and the analytical results. The uncertainty of the total deadtime is the uncertainties from group, veto and OR added in quadrature.

Q^2 (GeV/c)^2	Path	fractional contribution			Total deadtime loss at 100μA
		Group	Veto	OR	
1.1	narrow	$(20.6 \pm 2.1)\%$	$(51.3 \pm 1.9)\%$	$(28.1 \pm 8.6)\%$	$(1.45 \pm 0.13)\%$
	wide	$(29.5 \pm 2.4)\%$	$(45.3 \pm 1.7)\%$	$(25.3 \pm 9.0)\%$	$(1.64 \pm 0.16)\%$
1.9	narrow	$(2.9 \pm 0.2)\%$	$(80.6 \pm 18.5)\%$	$(16.5 \pm 12.3)\%$	$(0.885 \pm 0.196)\%$
	wide	$(4.3 \pm 0.4)\%$	$(76.6 \pm 17.5)\%$	$(19.1 \pm 15.1)\%$	$(0.931 \pm 0.215)\%$

the final asymmetry results from the wide path triggers are $(1.64 \pm 0.16)\%$ and $(0.931 \pm 0.215)\%$, for $Q^2 = 1.1$ and 1.9 (GeV/c)^2, respectively. These provide a direct correction to the measured asymmetry and the uncertainties are smaller than the 30% limit originally designed for this experiment.

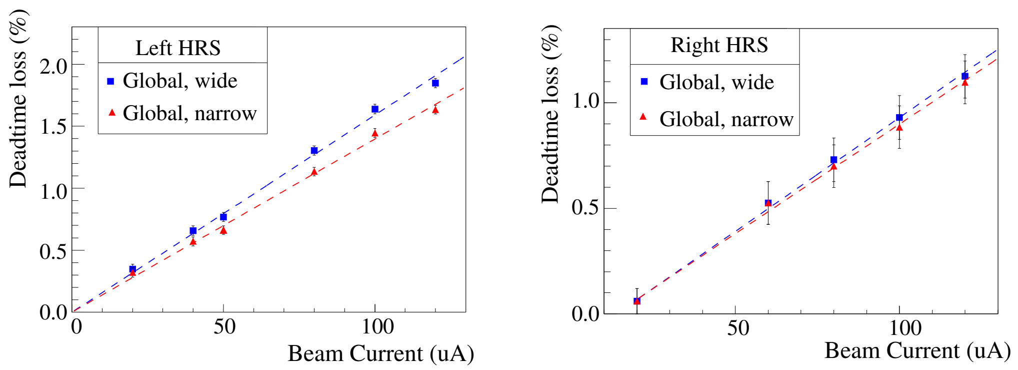

Fig. 8. [*Color online*] Simulated deadtime loss of the global electron trigger for the Left (left) and the Right (right) HRS. The error bars shown are due to statistical uncertainty of the simulation. See Table 1 for final uncertainty evaluation.

4.3 Asymmetries

The physics asymmetries sought for in this experiment are 90 and 160 ppm, for $Q^2 = 1.1$ and 1.9 (GeV/c)^2, respectively. The measured asymmetries are about 90% of these values due to beam polarization. To understand the systematics of the asymmetry measurement, a half-wave plate (HWP) was inserted in the beamline to flip the laser helicity in the polarized source during half of the data taking period. The measured asymmetries flip sign for each beam HWP change and the magnitude of the asymmetry remain consistent within statistical error bars.

The asymmetries can be formed from event counts of each beam helicity pair, with 33-ms of helicity right and 33-ms of helicity left beam, normalized by the beam charge. Figure 9 shows the pull distribution of pair-wise asymmetries with the "pull" defined as

$$p_i \equiv (A_i - \langle A \rangle)/\delta A_i \,, \tag{7}$$

where A_i is the asymmetry extracted from the i-th beam helicity pair with the HWP states already corrected and $\delta A_i = 1/\sqrt{N_i^R + N_i^L}$ its statistical uncertainty with $N_i^{R(L)}$ the event counts from the right (left) helicity pulse of the pair, and $\langle A \rangle$ is the asymmetry averaged over all beam pairs. One can see that the asymmetry spectrum agrees to five orders of magnitude with Gaussian distribution expected from purely statistical fluctuations.

5 Summary

A scaler-based counting DAQ with hardware-based particle identification was successfully implemented in the 6 GeV PVDIS experiment at Jefferson Lab. Asymmetries measured by the DAQ follow Gaussian distributions as expected from purely statistical measurements. Particle identification performance of the DAQ were measured during the experiment and corrections are applied to the data on a day-to-day basis. DAQ deadtime was calculated from a full-scale timing simulation and results are well understood. Systematic uncertainties from the new DAQ contribute to $\approx 0.2\%$ to the final asymmetry results and are negligible compared to the $(3-4)\%$ statistical uncertainty and other leading systematic uncertainties.

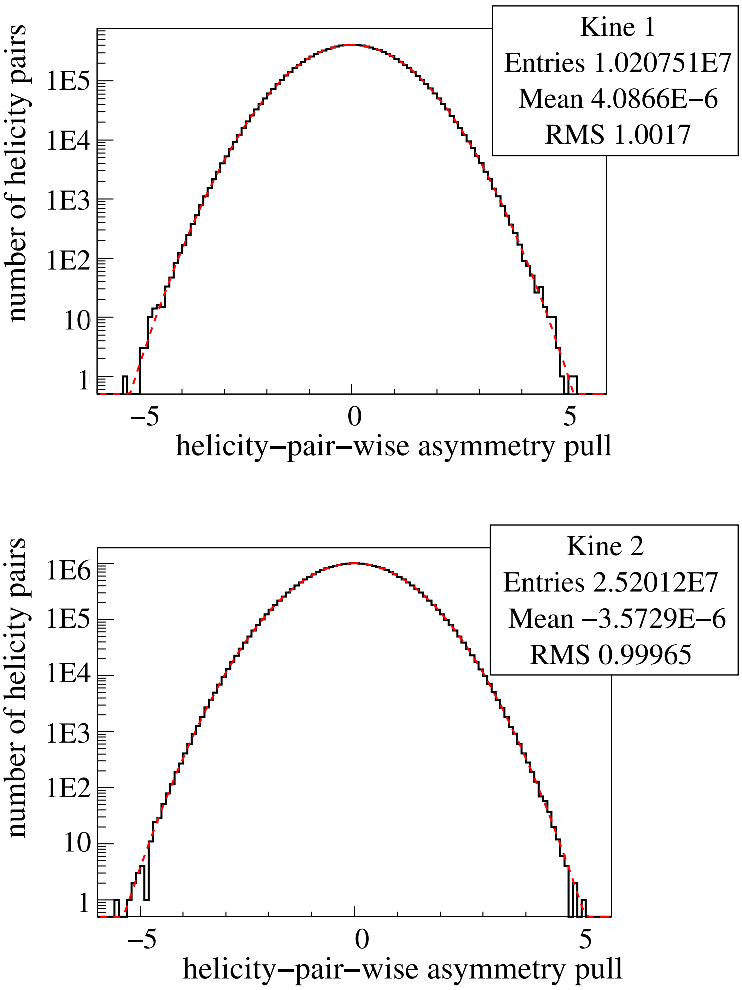

Fig. 9. [*Color online*] Pull distribution [Eq.(7)] for the global electron narrow trigger for $Q^2 = 1.1$ (top) and $Q^2 = 1.9$ (GeV/c)^2 (bottom).

Acknowledgments

This work is supported in part by the Jeffress Memorial Trust under Award No. J-836, the U.S. National Science Foundation under Award No. 0653347, and the U.S. Department of Energy under Award No. DE-SC0003885. **Notice:** Authored by Jefferson Science Associates, LLC under U.S. DOE Contract No. DE-AC05-06OR23177. The U.S. Government retains a non-exclusive, paid-up, irrevocable, world-wide license to publish or reproduce this manuscript for U.S. Government purposes.

References

[1] JLab experiment E08-011 (previously E05-007), R. Michaels, P.E. Reimer and X.-C. Zheng, spokespersons.

[2] R. Subedi *et al.*, AIP proceedings of the 18^{th} International Spin Physics Symposium (2009) 245.

[3] C.Y. Prescott *et al.*, Phys. Lett. **B77** (1978) 347.

[4] C.Y. Prescott *et al.*, Phys. Lett. **B84** (1979) 524.

[5] J. Alcorn *et al.*, Nucl. Instrum. Meth. **A522** (2004) 294.

[6] SLAC proposal E-149 P.E. Bosted *et al.*, spokesperons.

[7] D. S. Armstrong and R. D. McKeown, to be published in Annual Reviews of Nuclear and Particle Science, [arXiv:1207.5238 [nucl-ex]].

[8] S. Abrahamyan, Z. Ahmed, H. Albataineh, K. Aniol, D. S. Armstrong, W. Armstrong, T. Averett and B. Babineau *et al.*, Phys. Rev. Lett. **108**, 112502 (2012) [arXiv:1201.2568 [nucl-ex]].

[9] Z. Ahmed *et al.* [HAPPEX Collaboration], Phys. Rev. Lett. **108**, 102001 (2012) [arXiv:1107.0913 [nucl-ex]].